*Int. J. Solids Structures* Vol. 21, No. 9, pp. 957–975, 1985
Printed in Great Britain.

0020–7683/85 $3.00 + .00


# CONTACT STRESSES IN PIN-LOADED ORTHOTROPIC PLATES

M. W. HYER
Department of Engineering Science and Mechanics, Virginia Polytechnic Institute and State University, Blacksburg, VA 24061

and

E. C. KLANG
Department of Theoretical and Applied Mechanics, University of Illinois, Champaign-Urbana, IL 61801

(*Received* 22 *May* 1984; *in revised form* 30 *October* 1984)

**Abstract**—A study to determine the effects of pin elasticity, friction, and clearance on the stresses near the hole in a pin-loaded orthotropic plate is described. The problem is modeled as a contact elasticity problem, the pin and the plate being two elastic bodies interacting through contact. This modeling is in contrast to previous works, by other investigators, which have assumed that the pin is rigid or that it exerts a known cosinusoidal radial traction on the hole boundary. Neither of these approaches explicitly involves a pin. A complex variable series, a collocation procedure, and iteration were used to obtain numerical results for a variety of plate and pin elastic properties and various levels of friction and clearance. Collocation was used to enforce the boundary conditions at a finite number of points around the hole boundary and iteration was used to find the contact and no-slip regions on the boundary. Details of the numerical scheme are discussed. The study shows that pin elasticity is not as important as clearance, friction, or the elastic properties of the plate in determining contact stresses.

## INTRODUCTION

Because of the widespread usage of fiber-reinforced composite materials in structures, there have been a number of studies to determine the stress distribution around a hole in a pin-loaded orthotropic plate[1–16]. The studies have been two-dimensional plane-stress analyses aimed at understanding the behavior of pinned and bolted connectors made of fiber-reinforced composite materials. While the plate has been modeled various ways, including finite-element[1, 5–8, 10, 12, 14–16] and elasticity[2–4, 9, 11, 13] approaches, none of the studies have directly addressed the pin, or more importantly, pin/hole interaction. For the most part, the investigations have assumed that either the pin was perfectly rigid[1–9, 13–15], or that the pin produced a known cosinusoidal radial traction on the hole boundary[11, 12, 16]. This latter assumption was first used by Bickley[17] in a study of isotropic plates. Although this has been shown to be a good approximation for isotropic plates[18], its applicability to orthotropic plates has not been checked. Neither approach requires an explicit pin model and each analysis reduces to a boundary value problem involving a single body, namely the plate. The purpose of the work reported on here was to explicitly model the pin and its interaction with the hole when determining the stresses around a hole in a pin-loaded orthotropic plate. The pin model includes pin elasticity, and friction and clearance between the pin and the hole. The problem involves two elastic bodies in contact and is much more difficult than the single-body problem. One major difficulty is that the regions of contact and no-contact between the pin and hole are unknown a priori and must be solved for as part of the analysis. In addition, the presence of friction complicates the problem because the slip and no-slip regions must also be determined as part of the analysis. While pin elasticity[10], friction[2, 3, 5, 7, 13, 14], and clearance[2, 3, 5, 15] have been included in previous analyses of this problem, no analysis has examined all three simultaneously. The one analysis which did include pin elasticity used finite elements to represent the pin and the plate, the pin transmitting forces to the plate through springs connecting the nodes of the pin and plate. In that study the effects of pin elasticity were never established.

The analysis here is based on formulating the elasticity problem in terms of complex variable theory. Both the pin and the plate are linearly elastic and the plate is infinite in extent. The pin loads the plate through a body force acting on the pin. A solution to the problem is obtained by a numerical scheme, namely a collocation procedure and iteration. The collocation procedure enforces interface and boundary conditions at the pin/hole boundary at a finite number of points. The iteration procedure is used to find the contact and no-slip regions. This study begins by formally stating the problem. The key steps in the method of solution, which depends on having elasticity solutions for the plate and pin to somewhat arbitrary boundary tractions, are then outlined. Following that, the major components in the elasticity solutions are presented. Next, the details of the collocation and iteration procedures are described. The number of collocation points, the iteration technique, the number of iterations, and solution accuracy are discussed. Finally, numerical results are presented. These results illustrate the effect of pin elasticity on the stresses around the hole and also indicate the importance of pin/hole friction and clearance on the stress calculations. The effects of the plate's elastic properties on the stresses are illustrated with the computations. The study closes with a brief discussion.

## STATEMENT OF THE PROBLEM

The plate's principal material axes are aligned with an $x$-$y$ coordinate system. The origin of the $x$-$y$ system is the center of the hole, as is the origin of a cylindrical $r$-$\theta$ coordinate system. The hole is of unit radius and the plate is of unit thickness. The pin loading the hole is isotropic and the net force the pin exerts on the hole is in the $x$-direction. The pin radius is $1 - \lambda$ and, due to loading the hole, the center of the pin moves a distance $\delta$. Figure 1 depicts the geometry and coordinate systems used in the analysis. Figure 2 illustrates the parameters $\lambda$ and $\delta$. The case of $\lambda$ equal to zero represents a perfectly-fitting pin. As will be seen, this is a special case. A $+\delta$ is in the direction of the $+x$ axis. Here $\delta$ is considered the independent loading parameter and it is known. The pin force to produce $\delta$ is determined as part of the analysis.

As the pin moves to the right, it contacts a portion of the hole. The extent of the contact region is unknown and the half contact arc is denoted as $\beta$. Due to friction

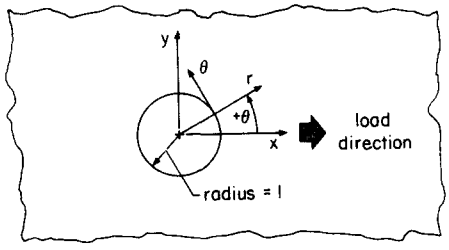


Fig. 1. Geometry and coordinate systems used in analysis.

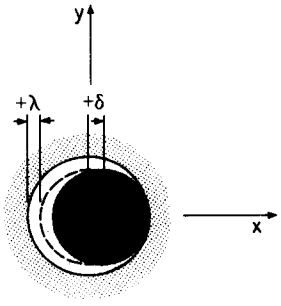


Fig. 2. Definition of clearance, $\lambda$, and pin displacement, $\delta$.

within the contact arc, there is a region of slip and a region of no-slip. The half no-slip arc is denoted as $\alpha$. Outside the region of contact there is a no-contact region. Figure 3 illustrates the various regions on the pin/hole boundary. Coulomb friction is assumed to act in the contact region. The coefficient of friction is denoted as $\mu$. It is assumed a priori that there is one contact region and within that region there is one no-slip region. It is conceivable that there might be multiple regions of contact and no-contact, or slip and no-slip. However, when the stresses are actually computed, the results can be examined for this possibility. If there are multiple regions of contact, tensile radial stresses will most likely develop in those regions where contact is erroneously assumed. For the cases considered there has been no evidence of this sort of behavior in the results. Also, examining the friction-induced shear stresses and their relation to the radial stresses will indicate whether multiple no-slip regions might occur. There has been no evidence of this behavior either. It is assumed that the coefficient of friction is independent of circumferential location. This assumption may not be as valid for composite materials as it would be, say, for metal.

Formally, the boundary and interface conditions between the plate and the pin can be stated as follows:

In region I, the no-slip region, $-\alpha \leqslant \theta \leqslant \alpha$:

$$u_{r_{\text{plate}}} = u_{r_{\text{pin}}} + \delta \cos(\theta) - \lambda \tag{1}$$

$$u_{\theta_{\text{plate}}} = u_{\theta_{\text{pin}}} - \delta \sin(\theta). \tag{2}$$

In region II, the slip regions, $\alpha < \theta \leqslant \beta$ and $-\beta \leqslant \theta < -\alpha$:

$$u_{r_{\text{plate}}} = u_{r_{\text{pin}}} + \delta \cos(\theta) - \lambda \tag{3}$$

$$|\tau_{r\theta}| = \mu |\sigma_r|. \tag{4}$$

In region III, the no-contact region, $\beta < \theta < 2\pi - \beta$:

$$\sigma_r = 0 = \tau_{r\theta} \tag{5), (6}$$

In the above, the radial and tangential elastic displacements of the pin and plate are given, respectively, by

$$u_{r_{\text{pin}}},\ u_{\theta_{\text{pin}}},\ u_{r_{\text{plate}}},\ u_{\theta_{\text{plate}}}.$$

Equations (1) and (3) express continuity of radial displacements in the contact region and eqn (2) expresses continuity of tangential displacements in the no-slip region. Equation (4) is the Coulomb friction law. Equations (5) and (6) express the traction-free conditions in the no-contact region. Because of the nature of friction, assumptions have to be made regarding the sign of $\tau_{r\theta}$. The problem can be solved assuming $\delta$ is increasing. This corresponds to a positive $\tau_{r\theta}$. Alternatively, the problem can be solved assuming $\delta$ is decreasing. This corresponds to a negative $\tau_{r\theta}$. Only the former condition will be discussed here.

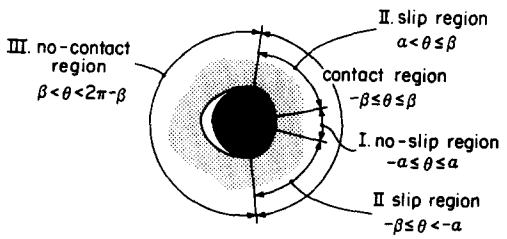


Fig. 3. Important regions at pin/hole boundary.

## METHOD OF SOLUTION

Due to equilibrium considerations, the boundary tractions acting on the pin are identical to the boundary tractions acting on the hole. As formulated here the problem reduces to finding these boundary tractions. Once the tractions are known, the stresses in the plate can be determined. Here the unknown boundary tractions are represented in the form of a complex Fourier series with unknown coefficients $A_k$. The series is given by

$$(N\text{-}iT)_{\text{pin}} = (N\text{-}iT)_{\text{plate}} = \sum_{-\infty}^{+\infty} A_k e^{ik\theta}, \text{ all } \theta, \tag{7}$$

where, following the convention of [19], $N$ is the normal, or radial, traction $\sigma_r$ on the boundary, and $T$ is the tangential, or shear, traction $\tau_{r\theta}$ on the boundary. Because the tangential tractions are odd functions of $\theta$ and the normal tractions are even functions of $\theta$, the $A_k$ are real.

Because each is a legitimate traction, each term $e^{ik\theta}$ in the series produces a unique set of stresses and displacements in the plate and in the pin. In the next sections, the stresses and displacements in the pin and plate due to traction $e^{ik\theta}$ will be determined. If the boundary traction is $A_k e^{ik\theta}$, then the stresses and displacements in the plate and pin will be weighted by $A_k$. If, for example, the radial displacement due to $N\text{-}iT = e^{ik\theta}$ is denoted as $(u_r)_k$, then the radial displacement due to traction $N\text{-}iT = A_k e^{ik\theta}$ is given by $A_k(u_r)_k$. Considering all terms in eqn (7), the radial displacement $u_r$ would be the weighted sum of the effects of the individual tractions $e^{ik\theta}$. That is,

$$u_r = \sum_{k=-\infty}^{\infty} A_k(u_r)_k. \tag{8}$$

If all $A_k$ were known, then $u_r$ could be calculated. The same can be said of the tangential displacement, namely

$$u_\theta = \sum_{k=-\infty}^{\infty} A_k(u_\theta)_k, \tag{9}$$

where $(u_\theta)_k$ is the tangential displacement due to traction $N\text{-}iT = e^{ik\theta}$. No distinction has yet been made between the plate and the pin. The responses of the plate due to $N\text{-}iT = e^{ik\theta}$ are different than the responses of the pin due to $N\text{-}iT = e^{ik\theta}$. Thus, the notation

$$u_{r_{\text{pin}}} = \sum_{k=-\infty}^{\infty} A_k(u_r)_{k\text{pin}}; \quad u_{\theta_{\text{pin}}} = \sum_{k=-\infty}^{\infty} A_k(u_\theta)_{k\text{pin}} \tag{10),(11}$$

$$u_{r_{\text{plate}}} = \sum_{k=-\infty}^{\infty} A_k(u_r)_{k\text{plate}}; \; u_{\theta_{\text{plate}}} = \sum_{k=-\infty}^{\infty} A_k(u_\theta)_{k\text{plate}} \tag{12),(13}$$

distinguishes between pin and plate responses. It is important to point out that, because they are a result of traction $e^{ik\theta}$, the quantities

$$(u_r)_{k\text{pin}}, (u_\theta)_{k\text{pin}}, (u_r)_{k\text{plate}}, \text{ and } (u_\theta)_{k\text{plate}}$$

are assumed to be known. The problem will reduce to finding $A_k$.

To continue with the formulation of the problem, the stresses in the pin and plate

are given by

$$\sigma_{r_{pin}} = \sum_{k=-\infty}^{\infty} A_k(\sigma_r)_{k_{pin}};\ \sigma_{r_{plate}} = \sum_{k=-\infty}^{\infty} A_k(\sigma_r)_{k_{plate}} \quad (14),(15)$$

$$\sigma_{\theta_{pin}} = \sum_{k=-\infty}^{\infty} A_k(\sigma_\theta)_{k_{pin}};\ \sigma_{\theta_{plate}} = \sum_{k=-\infty}^{\infty} A_k(\sigma_\theta)_{k_{plate}} \quad (16),(17)$$

$$\tau_{r\theta_{pin}} = \sum_{k=-\infty}^{\infty} A_k(\tau_{r\theta})_{k_{pin}};\ \tau_{r\theta_{plate}} = \sum_{k=-\infty}^{\infty} A_k(\tau_{r\theta})_{k_{plate}}. \quad (18),(19)$$

The quantities $(\sigma_r)_{k_{pin}}, \ldots, (\tau_{r\theta})_{k_{plate}}$ are the stresses in the pin and plate due to traction $N\text{-}iT = e^{ik\theta}$. They are also considered known.

To determine the unknown coefficients $A_k$, a collocation technique and iteration are used. Instead of using infinite sums in eqns (10–19), finite sums are used. Instead of satisfying the boundary conditions given by eqns (1–6) at each point on the circular boundary, (i.e., at an infinite number of points) the boundary conditions are satisfied at a finite number of points. The number of terms in the truncated series is related to the number of collocation points on the boundary. The iterative portion of the solution involves finding the contact and no-slip arcs, $\alpha$ and $\beta$. They, like the $A_k$, are unknown. However, if specific values are assumed for $\alpha$ and $\beta$, a solution to the problem with those values of $\alpha$ and $\beta$ can be found. The specific values may not yield a solution which satisfies all the boundary and interface conditions, but iteration can be used to find values which do satisfy all the conditions of the problem. The iteration procedure will be further discussed. First, the collocation procedure is explained.

By using finite sums in eqns (10–19) and substituting those sums into the boundary conditions for the various regions, eqns (1–6), the method for determining the $A_k$'s becomes evident. Substituting the finite sums into eqns (1–6) results in:

For the no-slip region;

$$\sum_{k=-M}^{M} A_k(u_r)_{k_{plate}} = \sum_{k=-M}^{M} A_k(u_r)_{k_{pin}} + \delta\cos(\theta) - \lambda \quad (20)$$

$$\sum_{k=-M}^{M} A_k(u_\theta)_{k_{plate}} = \sum_{k=-M}^{M} A_k(u_\theta)_{k_{pin}} - \delta\sin(\theta). \quad (21)$$

For the slip regions;

$$\sum_{k=-M}^{M} A_k(u_r)_{k_{plate}} = \sum_{k=-M}^{M} A_k(u_r)_{k_{pin}} + \delta\cos(\theta) - \lambda \quad (22)$$

$$\sum_{k=-M}^{M} A_k((\tau_{r\theta})_k - \mu(\sigma_r)_k) = 0. \quad (23)$$

For the no contact region;

$$\sum_{k=-M}^{M} A_k(\sigma_r)_k = 0, \quad (24)$$

$$\sum_{k=-M}^{M} A_k(\tau_{r\theta})_k = 0. \quad (25)$$

There are $2M + 1$ terms in each sum. If the boundary conditions are satisfied at $2M + 1$ discrete points around the circular boundary, a set of $2M + 1$ linear algebraic

equations can be formed from which to solve for the $A_k$. Since the proper symmetry conditions have been incorporated into the solution, the $2M + 1$ discrete points need only to be distributed over one-half the hole circumference, $0 \leq \theta \leq \pi$. The assumed values of $\alpha$ and $\beta$ determine over what range of $\theta$ eqns (20) and (21) are enforced, over what other range eqns (22) and (23) are enforced, and over what range eqns (24) and (25) are enforced. Because the tractions on the plate and pin are identical, neither the plate nor the pin is called out specifically in eqns (24) and (25). Although it is not specifically noted, attention must be given to signs in eqn (23). In addition, strictly speaking, by eqn (7)

$$(\sigma_r)_{k_{\text{pin}}} = (\sigma_r)_{k_{\text{plate}}} = \cos(k\theta) \quad \left.\right\} \text{at the} \tag{26}$$

and

$$(\tau_{r\theta})_{k_{\text{pin}}} = (\tau_{r\theta})_{k_{\text{plate}}} = -\sin(k\theta). \quad \left.\right\} \text{boundary} \tag{27}$$

Equations (23–25) thus can be written as

$$\sum_{k=-M}^{M} A_k \left(\sin(k\theta) + \mu \cos(k_\theta)\right) = 0. \tag{23a}$$

$$\sum_{k=-M}^{M} A_k \cos(k\theta) = 0 \tag{24a}$$

$$\sum_{k=-M}^{M} A_k \sin(k\theta) = 0. \tag{25a}$$

Expanding eqns (20–22) and (23a–25a), evaluating them at $2M + 1$ circumferential, $\theta$, locations, rearranging slightly, and putting them into matrix notation leads to $2M + 1$ equations of the form

$$[C]\{A\} = \{B\}. \tag{28}$$

The entries in the coefficient matric $[C]$ consist of terms involving $(u_r)_{0_{\text{plate}}}$, $(u_r)_{0_{\text{pin}}}$, $(u_r)_{-1_{\text{plate}}}$, . . . , $(u_\theta)_{M_{\text{pin}}}$, $\sin(\theta)$, and $\cos(\theta)$ evaluated at various $\theta$ locations around the hole circumference. The vector $\{B\}$ consists of terms of the form $(\delta \cos(\theta) - \lambda)$ and $(-\delta \sin(\theta))$ evaluated at various $\theta$ locations around the hole circumference. It is important to point out that with a perfectly fitting pin, $\lambda = 0$ and each element of $\{B\}$ of eqn 28 changes, for example, by a factor of two when $\delta$ is doubled. Each $A_k$ simply doubles and the spatial variation of *N-iT*, with $\theta$, remains unchanged. Thus $\alpha$ and $\beta$ are unaffected by $\delta$. With $\lambda \neq 0$, doubling $\delta$ does not result in a doubling of the right-hand side of eqn 28. Each $A_k$ changes by a different amount and thus the spatial variation of *N-iT* varies. This translates into $\delta$ directly affecting $\alpha$ and $\beta$. The perfect fit case is, therefore, quite special, and is often referred to as the linear case.

To implement the solution procedure the responses of the plate and pin to boundary traction $e^{ik\theta}$ namely $(u_r)_{k_{\text{pin}}}$, $(u_r)_{k_{\text{plate}}}$, $(u_\theta)_{k_{\text{pin}}}$, $(u_\theta)_{k_{\text{plate}}}$, $k = 0, \pm 1, \ldots, \pm M$ must be found. This follows.

## RESPONSE OF PIN TO $e^{ik\theta}$

In reality, the pin transmits a load to the hole boundary because it is loaded by some external mechanism. Commonly, the pin is in double shear, being loaded by two other plates parallel to and on either side of the plate under discussion. This is shown in Fig. 4a. To be sure, there are bending stresses in the pin and the exact determination of stresses in the pin requires a three-dimensional analysis. However, for the segment of pin within the thickness of the plate, the situation shown in Fig. 4b is quite accurate. This segment of the pin, shown as a disk, is loaded by shear stresses from portions of

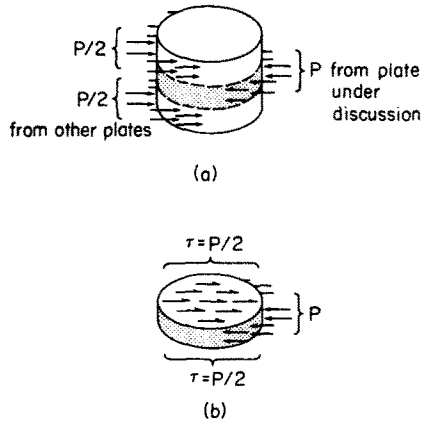


Fig. 4. Idealization of pin load: a) pin in double shear; b) section of pin within plate thickness.

the pin on either side of the plate, and by the contact stresses. Compared to the length of the pin, the region of the pin within the thickness of the plate is small. However, the fact that the pin actually has length does influence the deformation of the pin within the thickness region. Here the pin is assumed to be in a state of plane deformation and the shear stresses in Fig. 4b are assumed to be spatially uniform over the pin cross-sectional area. Furthermore, for purposes of analysis, the effects of the uniform shear traction are assumed to be equivalent to a uniformly distributed body force acting in the $x$ direction with the pin. An alternative pin model would be to assume the disk representing the pin is loaded at its center by a concentrated force. This model was not considered because it was felt to be too harsh an idealization of the forces actually transmitted to the portion of the pin within the thickness of the plate. A concentrated force model was adapted by Rao[20] in a study of isotropic plates.

With the model adopted here, the equilibrium equations for the pin are

$$\frac{\partial \sigma_r}{\partial r} + \frac{1}{r}\frac{\partial \tau_{r\theta}}{\partial \theta} + \frac{\sigma_r - \sigma_\theta}{r} + b_r = 0, \quad \frac{1}{r}\frac{\partial \sigma_\theta}{\partial \theta} + \frac{\partial \tau_{r\theta}}{\partial r} + \frac{2\tau_{r\theta}}{r} + b_\theta = 0, \quad \text{(29)a,(29)b}$$

where $b_r$ and $b_\theta$ are the components of the body force. Milne-Thompson[21] discusses the complex variable approach for the case of a body force, and so only the final results of the analysis are presented here. Details can be found in [22].

The first and second fundamental stress combinations for the pin are written as

$$\sigma_\theta + \sigma_r = 2(\Phi(z) + \overline{\Phi}(\bar{z})) + b_x\left(\frac{\kappa}{2} - 1\right)(z + \bar{z}), \tag{30}$$

$$\sigma_\theta - \sigma_r + i2\tau_{r\theta} = 2\left(\bar{z}\Phi'(z) + \Psi(z) + \kappa\frac{b_x}{4}\bar{z}\right)e^{i2\theta}, \tag{31}$$

and the elastic displacements are given as

$$(u_r + iu_\theta) = \frac{1}{2G}\left((3 - 4\nu)\phi(z) - z\overline{\phi}'(\bar{z}) - \overline{\psi}(\bar{z}) - \kappa\frac{b_x}{8}(z^2 + 2z\bar{z})\right)e^{-i\theta}. \tag{32}$$

In the above, the prime, ', denotes differentiation with respect to the argument, $G$ is the material's shear modulus, and

$$\Phi(z) = \phi'(z), \ \Psi(z) = \psi'(z), \quad \text{and} \quad \psi(z) = \chi'(z). \tag{33a,b,c}$$

The functions $\phi(z)$ and $\psi(z)$ are analytic functions of $z$, $z = x + iy = re^{i\theta}$. The overbar, $\bar{}$, denotes complex conjugate. The quantity $b_x$ is the body force in the $x$ direction and

it is given by

$$b_x = \sqrt{b_r^2 + b_\theta^2}. \tag{34}$$

At the boundary

$$\sigma_r - i\tau_{r\theta} = N - iT = \sum_{k=-\infty}^{\infty} A_k e^{ik\theta}. \tag{35}$$

Therefore the stress combination most useful for matching traction boundary conditions is obtained by subtracting eqn (31) from eqn (30). The result is

$$\sigma_r - i\tau_{r\theta} = \Phi(z) + \overline{\Phi}(\bar{z}) - (\bar{z}\Phi'(z) + \Psi(z))e^{i2\theta} - \frac{b_x}{4}(2 - \kappa)(z + \bar{z}) - \kappa\frac{b_x}{4}\bar{z}e^{i2\theta}. \tag{36}$$

Because the pin domain is simply connected, $\Phi(z)$ and $\Psi(z)$ can be represented by

$$\Phi(z) = \sum_{k=0}^{\infty} a_k z^k = \sum_{k=0}^{\infty} a_k r^k e^{ik\theta} \tag{37a}$$

$$\Psi(z) = \sum_{k=0}^{\infty} b_k z^k = \sum_{k=0}^{\infty} b_k r^k e^{ik\theta}, \tag{37b}$$

$a_k$ and $b_k$ being constants, possibly complex.

Substituting eqn (37) into eqns (30–32), the stresses and displacements can be determined in terms of $a_k$, $b_k$, and $b_x$. Specifically, the stress combination of eqn (36) evaluated on the boundary is

$$\sum_{k=-\infty}^{\infty} A_k e^{ik\theta} = \sum_{k=0}^{\infty} a_k R^k e^{ik\theta} + \sum_{k=0}^{\infty} \bar{a}_k R^k e^{-ik\theta} - \sum_{k=1}^{\infty} k a_k R^k e^{ik\theta} - \sum_{k=2}^{\infty} b_{k-2} R^{k-2} e^{ik\theta} - \frac{b_x R(2 - \kappa)}{4}(e^{i\theta} + e^{-i\theta}) - \frac{b_x R\kappa}{4} e^{i\theta}. \tag{38}$$

Here $R$ is the radius of the pin. Since the hole in the plate is of unit radius and the clearance between the pin and hole is $\lambda$,

$$R = 1 - \lambda. \tag{39}$$

Using eqn (38) and setting all $A_k$'s to zero except one, and setting that $A_k$ equal to one, constants $a_k$ and $b_k$ can be found by matching terms on the left and right sides of eqn (38). The solution of the pin to traction $N - iT = e^{ik\theta}$ is now available. This solution, in turn, is used in forming part of the entries of $[C]$ in eqn (28).

It should be mentioned that $b_x$ is not an independent constant. The body force and the boundary tractions must be in equilibrium. Except for $k = +1$, boundary tractions of the form $e^{ik\theta}$ do not produce a net force on the boundary. Therefore, $b_x$ is identically zero except for the case when $A_1$ is nonzero. For the boundary traction $A_1 e^{i\theta}$,

$$b_x = \frac{2A_1}{R}. \tag{40}$$

It should also be mentioned that, in determining the results here, the imaginary part of $a_0$ was arbitrarily assumed to be zero.

## RESPONSE OF PLATE TO $e^{ik\theta}$

The plate is assumed to be in a state of plane stress with tractions of the form

$$N - iT = \sum_{k=-\infty}^{\infty} A_k e^{ik\theta}$$

acting on the hole boundary. These surface tractions are in equilibrium with vanishingly small stresses at infinity. The plate's principal material axes are aligned with the $x$ and $y$ axes and so the constitutive behavior can be written as

$$\begin{Bmatrix} \epsilon_x \\ \epsilon_y \\ \gamma_{xy} \end{Bmatrix} = \begin{bmatrix} \frac{1}{E_x} & -\frac{\nu_{xy}}{E_x} & 0 \\ -\frac{\nu_{xy}}{E_x} & \frac{1}{E_y} & 0 \\ 0 & 0 & \frac{1}{G_{xy}} \end{bmatrix} \begin{Bmatrix} \sigma_x \\ \sigma_y \\ \tau_{xy} \end{Bmatrix}. \tag{41}$$

Here $E_x$ and $E_y$ are Young's moduli in the $x$ and $y$ directions, respectively, $\nu_{xy}$ is the Poisson's ratio relating contraction in the $y$ direction to the extension in the $x$ direction caused by a tensile stress in the $x$ direction, and $G_{xy}$ is the shear modulus in the $x$-$y$ plane. The equilibrium equations in the principal material system are

$$\frac{\partial \sigma_x}{\partial x} + \frac{\partial \tau_{xy}}{\partial y} = 0; \qquad \frac{\partial \tau_{xy}}{\partial x} + \frac{\partial \sigma_y}{\partial y} = 0. \tag{42}$$

Defining a stress function as

$$\sigma_x = \frac{\partial^2 F}{\partial y^2}; \qquad \sigma_y = \frac{\partial^2 F}{\partial x^2}; \qquad \tau_{xy} = -\frac{\partial^2 F}{\partial x \partial y}, \tag{43}$$

the equilibrium equations are satisfied. Using the constitutive equations and the stress function, the only nontrivial compatibility equation can be used to determine $F$. This equation is

$$\frac{\partial^4 F}{\partial y^4} + \left(\frac{E_x}{G_{xy}} - 2\nu_{xy}\right) \frac{\partial^4 F}{\partial x^2 \partial y^2} + \frac{E_x}{E_y} \frac{\partial^4 F}{\partial x^4} = 0. \tag{44}$$

Lekhnitskii[23] and Milne-Thompson[21] discuss the general solution to this equation and associated boundary conditions, while de Jong[4, 9, 13], Oplinger and Gandhi[2, 3], and Mangalgiri[7] discuss the solution in the context of a plate with a hole. Therefore, details of the solution are omitted here. Details can be found in [22].

The solution to eqn (44) has the form

$$F = \frac{1}{4}[W_1(z_1) + W_2(z_2) + \overline{W}_1(\overline{z}_1) + \overline{W}_2(\overline{z}_2)], \tag{45}$$

where

$$z_1 = x + \mu_1 y \quad \text{and} \quad z_2 = x + \mu_2 y \tag{46}$$

and $\mu_1$ and $\mu_2$ are two roots of the characteristic equation associated with eqn (44). With the change of variables, new nomenclature can be introduced, namely,

$$W_k'(z_k) = W_k'(z_k(\zeta_k)) \equiv 2\phi_k(\zeta_k), \qquad k = 1, 2. \tag{47}$$

where

$$\begin{aligned} \zeta_1 &= \frac{z_1 + \sqrt{z_1^2 - 4\gamma_1\delta_1}}{2\gamma_1} \\ \zeta_2 &= \frac{z_2 + \sqrt{z_2^2 - 4\gamma_2\delta_2}}{2\gamma_2}. \end{aligned} \tag{48}$$

The functions $\phi_k(\zeta_k)$ are of the form

$$\begin{aligned} \phi_1(\zeta_1) &= a_0 \ln \zeta_1 + \sum_{k=1}^{\infty} \frac{a_k}{\zeta_1^k} \\ \phi_2(\zeta_2) &= b_0 \ln \zeta_2 + \sum_{k=2}^{\infty} \frac{b_k}{\zeta_2^k}, \end{aligned} \tag{49}$$

where the $a_k$'s and $b_k$'s are constants. The logrithmic terms reflect the fact that there is a net force on the boundary of the singly connected plate.

For the plate the analog to eqn (36), evaluated on the hole boundary, becomes

$$\begin{aligned} \sum_{k=-\infty}^{\infty} A_k e^{ik\theta} &= \bar{\delta}_1\left(\bar{a}_0 e^{i\theta} - \sum_{k=1}^{\infty} k\bar{a}_k e^{i(k+1)\theta}\right) + \\ \bar{\delta}_2\left(\bar{b}_0 e^{i\theta} - \sum_{k=1}^{\infty} k\bar{b}_k e^{i(k+1)\theta}\right) &- \gamma_1\left(a_0 e^{i\theta} - \sum_{k=1}^{\infty} k a_k e^{-i(k-1)\theta}\right) \\ &- \gamma_2\left(b_0 e^{i\theta} - \sum_{k=1}^{\infty} k b_k e^{-i(k-1)\theta}\right). \end{aligned} \tag{50}$$

As in the procedure for the pin, setting all $A_k$ to zero except one gives equations for determining $a_k$ and $b_k$, and hence the response of the plate to traction $N\text{-}iT = e^{ik\theta}$ on the hole. However, with the plate, the procedure is slightly different. No matter which $A_k$ is being considered, eqn (50) always yields an equation for $a_0$ and $b_0$, in addition to other equations involving other $a$'s and $b$'s. This equation is

$$\bar{\delta}_1\bar{a}_0 + \bar{\delta}_2\bar{b}_0 - \gamma_1 a_0 - \gamma_2 b_0 = \begin{cases} 1, & \text{when } A_1 = 1 \\ 0, & \text{all other cases.} \end{cases} \tag{51}$$

More information is needed to determine $a_0$ and $b_0$. The information can be obtained by enforcing single-valuedness of the displacements. This issue is raised because of the logrithmic term in eqn (49) and

$$(u_r + iu_\theta)_{\theta=0} = (u_r + iu_\theta)_{\theta=2\pi} \tag{52}$$

must be satisfied.

With the response of the plate to the traction $N - iT = e^{ik\theta}$ available, these responses can be used to form the remainder of $[C]$ in eqn (28).

## DETAILS OF THE NUMERICAL SCHEME

The collocation procedure included the points $\theta = 0$ and $\theta = \pi$. Because of symmetry, the elasticity solutions for the pin and the plate due to traction $N\text{-}iT = e^{ik\theta}$

automatically yielded

$$(u_\theta)_{k_{pin}} = (u_\theta)_{k_{plate}} = 0 \text{ at } \theta = 0,\ k = 0, \pm 1, \ldots, \pm N. \tag{53}$$

and

$$(\tau_{r\theta})_{k_{pin}} = (\tau_{r\theta})_{k_{plate}} = 0 \text{ at } \theta = \pi,\ k = 0, \pm 1, \ldots, \pm N. \tag{54}$$

These two conditions led to two columns and rows of eqn (28) being zero. The collocation procedure included points at $\theta = 0$ and $\theta = \pi$ because there was one other condition at each point that had to be enforced, namely

$$(u_r)_{pin} = (u_r)_{plate} - \delta \text{ at } \theta = 0 \tag{55}$$

and

$$\sigma_r = 0 \text{ at } \theta = \pi. \tag{56}$$

Thus, the two rows and columns representing eqns (53) and (54) were eliminated from the set of linear equations, eqn (28). Failure to do this resulted in a singular matrix. The number of equations and unknown $A_k$'s solved for was reduced to $2M - 1$.

Values for $\alpha$, $\beta$, and $\delta$ were chosen. The system of $2M - 1$ equations was solved for the $A_k$'s. In all likelihood, the values of $\alpha$ and $\beta$ chosen did not satisfy all the interface and boundary conditions for that specific value of $\delta$. An iterative process then began to find values of $\alpha$ and $\beta$ that did. The key to the iteration process was the satisfaction of conditions stipulated by eqns (4–6).

To obtain a solution, the value of $\alpha$ was set to a value corresponding to the first collocation point away from $\theta = 0$. Attention was focused on $\beta$ by selecting a realistic value. Depending on whether the value of $\beta$ chosen was larger or smaller than the correct value, the $\sigma_r$ vs. $\theta$ relation had very distinctive characteristics near $\theta = \beta$. Figure 5 illustrates the nature of the solution for three values of $\beta$. The correct value of $\beta$ is denoted $\beta^*$. If the value of $\beta$ chosen was larger than $\beta^*$, say $\beta = \beta_1$, $\sigma_r$ was tensile near $\theta = \beta_1$. If the value of $\beta$ chosen was smaller than $\beta^*$, say $\beta = \beta_2$, then $\sigma_r$ was not zero at $\theta = \beta_2$. By recognizing what the character of the $\sigma_r$ vs. $\theta$ meant relative to the assumed value of $\beta$, within 3 or 4 iterations a value of $\beta$ could be obtained which satisfied eqns (5) and (6). Iteration for $\alpha$ then began. This iteration procedure was similar in that the $\tau_{r\theta}$ vs. $\theta$ relation showed distinct characteristics near $\theta = \alpha$. These characteristics depended on whether the value of $\alpha$ chosen was larger or smaller than the correct $\alpha$. The characteristics near $\theta = \alpha$ are shown in Fig. 6. The correct

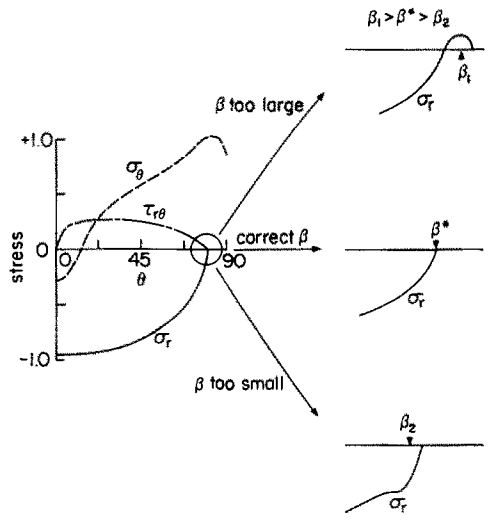


Fig. 5. Choosing the correct value of $\beta$.

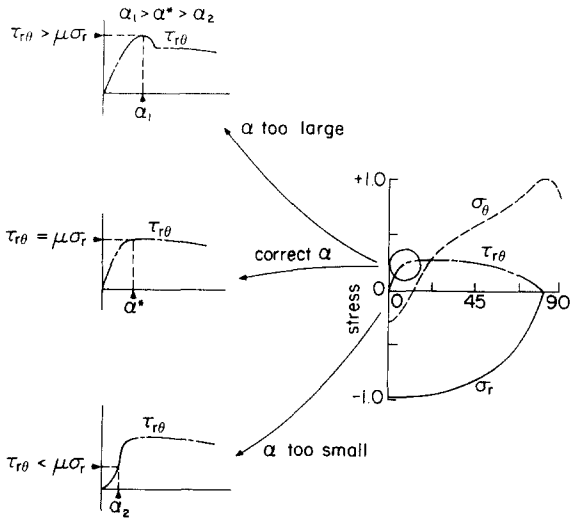


Fig. 6. Choosing the correct value of $\alpha$.

value of $\alpha$ is denoted as $\alpha^*$. If the value of $\alpha$ chosen was larger than $\alpha^*$, say $\alpha_1$, then at $\theta = \alpha_1$, $|\tau_{r\theta}|$ exceeded $\mu |\sigma_r|$. If the value of $\alpha$ chosen was smaller than $\alpha^*$, say $\alpha = \alpha_2$, then at $\theta = \alpha_2$, $|\tau_{r\theta}|$ was less than $\mu |\sigma_r|$. Within 3 or 4 iterations, a solution for $\alpha$ was obtained which satisfied eqn (4). The value of $\beta$ was then rechecked and adjusted if necessary. Generally, there was little coupling between the two variables.

For smaller values of $\mu$ (e.g. $\mu = 0.2$) the no-slip region was found to be small. Often the no-slip region was smaller than the spacing between the collocation point at $\theta = 0$ and the point next to it. In these cases the no-slip condition was satisfied only at $\theta = 0$. Since, by the symmetric nature of the solution there was no relative tangential motion at $\theta = 0$ anyway, the no-slip region could only be determined to be less than the collocation point spacing.

Forty collocation points around the half-circle were used to obtain the numerical results presented in the next section. Thus the results to be presented used 78 unknown $A_k$'s in the series representing *N-iT*. The 78 terms were divided evenly between negative $k$ and positive $k$. Twenty to 30 collocation points gave reasonable results when compared to similar cases from previous investigations. Forty points represented the upper limit of the interactive computer used in the analysis. Fewer than 20 points resulted in poor agreement with established work, e.g. rigid pin results.

## NUMERICAL RESULTS

Numerical results were obtained in order to assess the effects of the various parameters on the stresses around the hole. The numerical study considered plates with varying degrees of orthotropy. The results for four different plates are presented here. In the context of fiber-reinforced composite plates, these four plates represent four different laminates. The material properties of each plate are indicated in Table 1, as are the laminates they represent. The plate properties considered coincide with the basic properties used by Crews *et al.*[10] and represent a graphite-epoxy material.

Plate *A* represents an extreme in degree of orthotropy. The plate is much stiffer in the load direction than it is perpendicular to the load direction. This represents a graphite-epoxy plate made with all the fibers in the direction of the load. Plate *B* represents the other extreme, being much softer in the load direction than perpendicular to the load direction. Plate *B* represents a graphite-epoxy plate with all the fibers perpendicular to the load direction. Plate *C* represents a plate with properties representative of laminates which have the same inplane stiffness in all directions. Such laminates are referred to as quasi-isotropic laminates. Plate *D* represents a moderately orthotropic laminate, being three times stiffer in the load direction than it is perpen-

Table 1. Material properties of plates.

| Plate | $E_x$ Msi | $E_y$ Msi | $G_{xy}$ Msi | $\nu_{xy}$ | Representative laminate* |
|---|---|---|---|---|---|
| A | 21.3 | 1.58 | 0.930 | 0.38 | 0° |
| B | 1.58 | 21.3 | 0.930 | 0.028 | 90° |
| C | 8.40 | 8.40 | 3.20 | 0.310 | $(0°/\pm 45°/90°)_s$ |
| D | 12.4 | 3.73 | 3.21 | 0.667 | $(0°_2/\pm 45°)_s$ |

[a] fiber angles relative to $+x$ direction

dicular to the load. These four plates will be used to illustrate the effect of pin flexibility and the plate's elastic properties on the stresses around the hole. Plate *D* then will be used to illustrate the effect of friction, clearance, and pin displacement on stresses.

Figures 7–10 show the effects of pin flexibility and plate material properties on the stresses around the hole. The three pin flexibilities used were: a rigid pin, a steel pin ($E = 30 \times 10^6$ psi), and an aluminum pin ($E = 10 \times 10^6$ psi). Poisson's ratio of the pin had very little effect on the numerical results and a value of 0.3 was used. In each of Figs. 7–10, the coefficient of friction between the plate and the pin was assumed to be 0.2. This represents a reasonable value for metal on graphite-epoxy. The nondimensional clearance between the pin and plate, $\lambda/R$, was 0.01, and the nondimensional pin displacement, $\delta/R$, was 0.035. Realistic values of pin/hole clearance vary from application to application but $\lambda/R = 0.01$ is representative. Each figure has the same scale, for easy comparison, and each figure illustrates the three stresses at the hole edge, i.e. the radial stress $\sigma_r$, the circumferential stress $\sigma_\theta$, and the friction-induced shear stress $\tau_{r\theta}$. The stresses have been nondimensionalized by the bearing stress and the behavior of the stresses with circumferential location is illustrated. The bearing stress *S* is defined as the pin load, *P*, divided by the product of plate thickness and hole diameter. Also shown in Figs. 7–10 is the cosinusoidal radial stress distribution often assumed. Thus, the figures illustrate the two assumed pin/hole interaction models used in previous investigations, i.e. rigid and cosinusoidal, as well as the current, more realistic one. As a check on the numerical solution, the stresses $\sigma_r$ and $\tau_{r\theta}$ were inte-

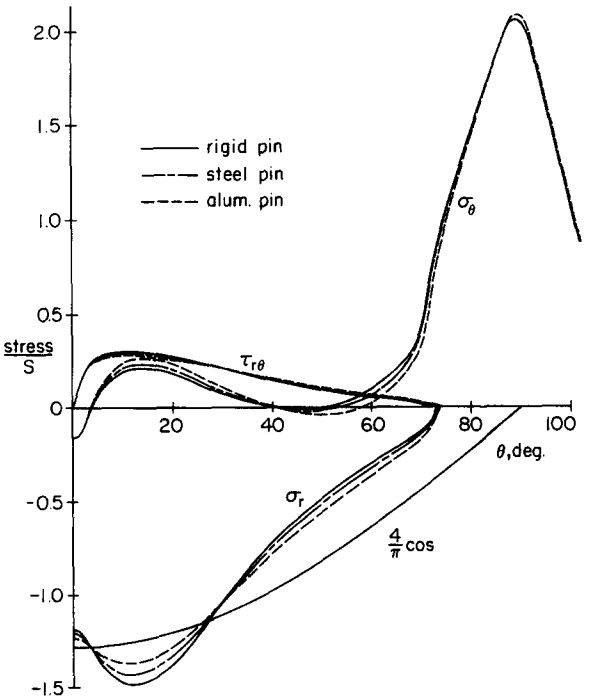


Fig. 7. Stresses around hole in plate *A*.

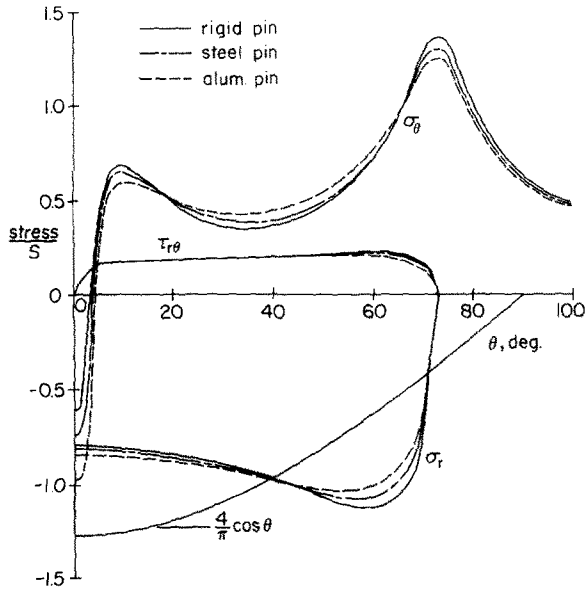


Fig. 8. Stresses around hole in plate *B*.

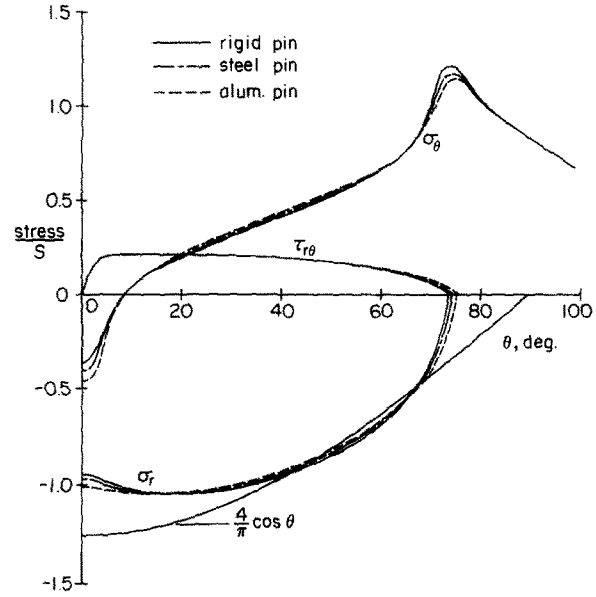


Fig. 9. Stresses around hole in plate *C*.

grated around the hole edge to determine the total load acting on the hole. The integration was always within 0.01% of *P*.

When examining Figs. 7–10, three conclusions are obvious. First, it is clear that pin flexibility is not a big factor in determining the stresses at the hole edge. Until now, no investigation has shown this explicitly. Second, the degree of orthotropy strongly influences the peak stresses and the distribution of the stresses around the hole. The highly orthotropic plate *A* in Fig. 7 has a stress concentration factor of 2 for the circumferential stress, compared to the 1.2 of the quasi-isotropic plate *C* in Fig. 9. Third, the often-assumed cosinusoidal distribution is not generally accurate. It is a serious misrepresentation for plate *B* and, due to pin/hole clearance effects, does not properly represent the contact region in any situation. It will be seen that the character of $\sigma_r$ near $\theta = 0$ is determined by friction, while the character of $\sigma_r$ near 90° is determined by pin/hole clearance. Thus, for particular friction and clearance levels, the cosinusoidal

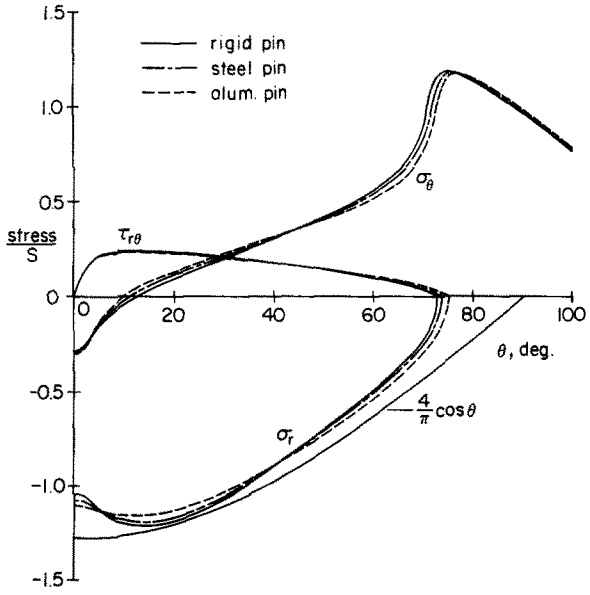


Fig. 10. Stresses around hole in plate *D*.

distribution could be a good representation. However, in all cases, the rigid pin assumption is better. In all the cases shown in Figs. 7–9, the circumferential stress $\sigma_\theta$ is negative at $\theta = 0$. This is somewhat counter to intuition, but the result, as will be seen shortly, is due to frictional effects. This was found in Wilkinson's[5] analysis and it has been measured[24, 25]. The decrease in the magnitude of $\sigma_r$ as $\theta \to 0$, in plate *A* for example, is also due to friction.

Table 2 indicates the contact and no-slip anlge determined by the iterative procedure for Figs. 7–10 and for figures to be discussed. The location of the maximum hoop stress is also indicated in the table. The location of the maximum hoop stress, while generally occurring near the end of the contact region, depends on the plate's elastic properties. A plate representing a laminate with fibers at $+45°$ and $-45°$ relative to the load direction experiences a maximum hoop stress at roughly $\theta = 45°$.

Figure 11 illustrates the effect of friction on the stresses at the hole edge of plate *D*. Three values of friction were examined for the case of a steel pin with clearance

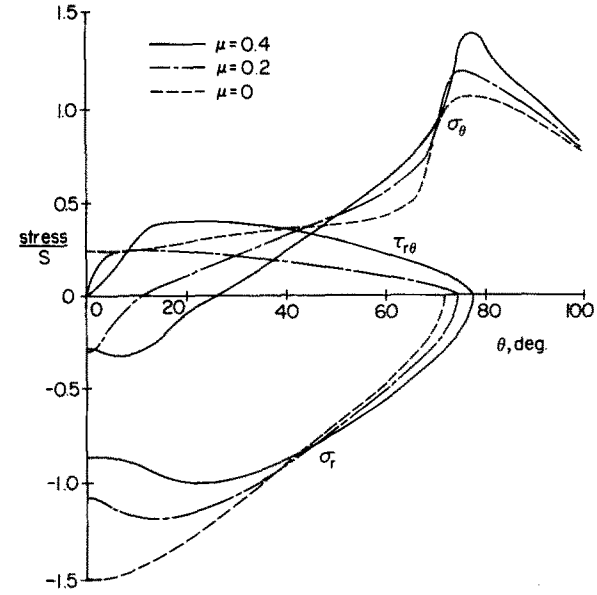


Fig. 11. Effect of friction on stresses.

Table 2. Location of maximum hoop stress, contact, and no-slip regions for various cases.

| Plate | Fig. No. | Fixed conditions | Variable condition | Location of max $\sigma_\theta$ | Contact arc, $\beta$ | No-slip arc, $\alpha$ |
|---|---|---|---|---|---|---|
| | | | pin | | | |
| | | $\mu = 0.2$ | rigid | 88° | 74° | $< 5°$ |
| A | 7 | $\delta/R = 0.035$ | steel | 88° | 74° | $< 5°$ |
| | | $\lambda/R = 0.01$ | aluminum | 88° | 74° | $< 5°$ |
| | | | pin | | | |
| | | $\mu = 0.2$ | rigid | 74° | 74° | $< 5°$ |
| B | 8 | $\delta/R = 0.035$ | steel | 74° | 74° | $< 5°$ |
| | | $\lambda/R = 0.01$ | aluminum | 74° | 74° | $< 5°$ |
| | | | pin | | | |
| | | $\mu = 0.2$ | rigid | 74° | 74° | $< 5°$ |
| C | 9 | $\delta/R = 0.035$ | steel | 74° | 74° | $< 5°$ |
| | | $\lambda/R = 0.01$ | aluminum | 76° | 76° | $< 5°$ |
| | | | pin | | | |
| | | $\mu = 0.2$ | rigid | 74° | 74° | $< 5°$ |
| D | 10 | $\delta/R = 0.035$ | steel | 74° | 74° | $< 5°$ |
| | | $\lambda/R = 0.01$ | aluminum | 76° | 75° | $< 5°$ |
| | | | $\mu$ | | | |
| | | steel pin | 0 | 76° | 71° | — |
| D | 11 | $\delta/R = 0.035$ | 0.2 | 74° | 74° | $< 5°$ |
| | | $\lambda/R = 0.01$ | 0.4 | 77° | 77° | 10° |
| | | | $\lambda/R$ | | | |
| | | $\mu = 0.2$ | 0 | 86° | 86° | $< 5°$ |
| D | 12 | steel pin | 0.01 | 74° | 74° | $< 5°$ |
| | | $\delta/R = 0.035$ | 0.02 | 69° | 56° | $< 5°$ |
| | | | $\delta/R$ | | | |
| | | $\mu = 0.2$ | 0.02 | 66° | 61° | $< 5°$ |
| D | 13 | steel pin | 0.035 | 74° | 74° | $< 5°$ |
| | | $\lambda/R = 0.01$ | 0.05 | 78° | 78° | $< 5°$ |

$\lambda/R = 0.01$ and displacement $\delta/R = 0.035$. The values of friction examined were: $\mu = 0$, 0.2, and 0.4. The first and third values of $\mu$ represent extremes and were chosen to bracket the effects of friction. The most significant effect of friction, besides influencing the level of shear stress, is its influence on peak stresses. Increasing friction tends to decrease the maximum radial stress at $\theta = 0$. This effect occurred for all situations studied. Friction also increased the maximum circumferential stress near the end of the contact region. Friction had some effect on the actual contact zone. Because of the effect of friction at $\theta = 0$, the cosinusoidal representation (not shown) is closer to the frictionless case than the other cases. In fact, with no friction and no clearance, the cosinusoidal assumption is close for this particular plate.

Figure 12 illustrates the effect of pin/hole clearance on the hole-edge stresses in plate *D*. The three levels of clearance illustrated are $\lambda/R = 0.0$, 0.01, 0.02. The value $\lambda/R = 0$ is often referred to as the snug-fit, push-fit, or perfect-fit pin. The value of $\mu$ used was 0.2 and $\delta/R$ was 0.035. The pin was steel. The most effect pin/hole clearance has is in the location of the peak circumferential stress. Increasing the clearance moves the peak stress location toward $\theta = 0$. This is a direct consequence of the rapid decrease in contact zone with increasing clearance. Increasing the clearance also causes more of a region to experience high circumferential stress. Table 2 quantifies the effect of clearance on contact angle. As expected, the value of the peak radial stress is sensitive to the level of clearance. With less contact area the pin naturally loads the contact region more.

Finally, Fig. 13 shows the effect of increasing pin displacement on the stresses. The pin is steel, the coefficient of friction is 0.2, and the clearance is 0.01. Three values of pin displacement are considered: $\delta/R = 0.02$, 0.035 and 0.05. The most significant effects are with the contact arc and the location of the peak circumferential stress. With increasing pin displacement, the contact arc increases and the location of the

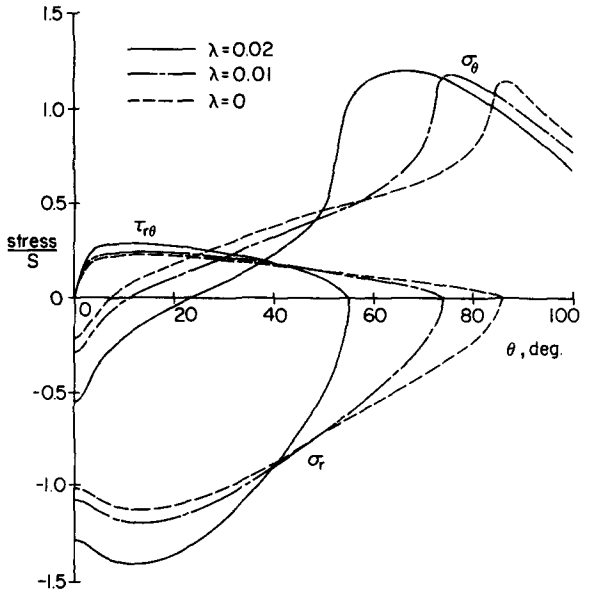


Fig. 12. Effect of clearance on stresses.

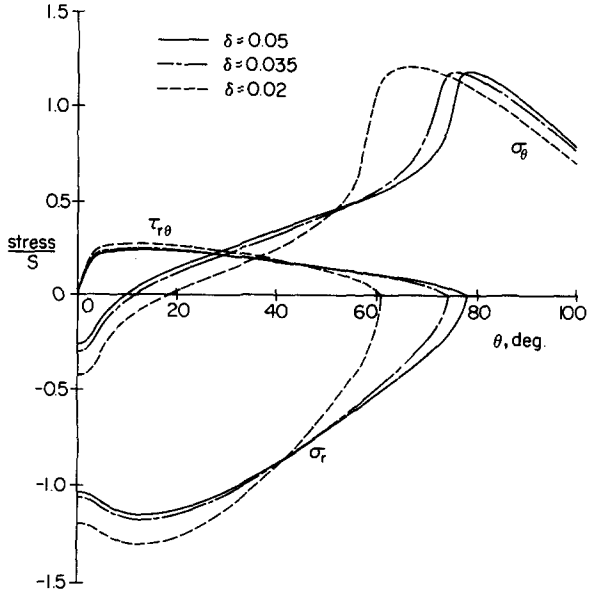


Fig. 13. Effect of pin displacement on stresses.

peak circumferential stress moves toward $\theta = 90°$. Obviously increasing pin displacement increases the magnitude of the actual stresses. However, in the nondimensional sense shown in Fig. 13, the stress magnitudes are not strongly influenced. The peak nondimensional radial stress actually decreases some with increasing pin displacement, due to the longer contact arc.

## ADDITIONAL COMMENTS

Two other issues should be addressed before closing. The first issue deals with the functional behavior of the stresses between collocation points. The second issue deals with friction.

Figures 7–13 were drawn by hand-fairing lines through the numerical values of the stresses computed at the collocation points. When a Fourier series representation of

a function is used in conjunction with collocation, there is the issue of behavior of the series representation between the collocation points. In addition, here, there is the issue of the behavior near the end of the contact zone, where the stress state is rapidly changing with $\theta$. When the numerical values of $A_k$ were substituted into eqn (7) and $N$ ($= \sigma_r$ at the hole edge), for example, was computed as a function of $\theta$, the function did, indeed, oscillate between collocation points. For a typical situation, for $\theta \leq \beta$ the amplitude of the oscillation was less than 2% of its maximum value. Just beyond $\theta = \beta$, the amplitude of the oscillation increased, but not markedly. Oscillation to a certain degree was expected. Wilson and Goree[26] discussed a dual-series approach to a contact problem which resulted in very little oscillation anywhere. Such an approach could have been used in this problem. However, nothing other than minimal oscillations were experienced with the numerical approach here and so the issue of other numerical schemes did not arise.

Concerning friction, Dundurs and Comninou[27] have shown that, at the transition point between no-slip and slip, the slope of $\tau_{r\theta}$, with respect to $\theta$, becomes infinite. With the approach here, such behavior would never be realized and thus the results are in error in that regard. An alternative approach would have been to build-in a special friction-induced shear function which did indeed yield an infinite slope of the transition point. However, it is felt that the results presented are not in error for not accurately representing this effect.

## CONCLUDING REMARKS

This study has used elasticity solutions and a numerical procedure to study the stress distributions around a hole in a pin-loaded orthotropic plate. In particular, the effects of pin elasticity, friction, and clearance have been studied. In addition, the effects of the plate's elastic properties on the stress distribution has been assessed. It can be concluded that, within the context of this study, pin elasticity is not an important variable. Pin/hole clearance is an important variable and friction does effect the stress distributions. Further studies are warranted in the area of finite-geometry plates, a circumferentially variable coefficient of friction, or alternatively, a more general (non-Coulomb) friction model. Perhaps experimental investigations into the slip and no-slip zones are necessary before more general friction laws are incorporated.

*Acknowledgements*—The work reported on here was supported by the NASA-Virginia Tech Composites Program, Cooperative Agreement NAG-1-343 with the NASA Langley Research Center.

## REFERENCES

1. J. P. Waszczak and T. A. Cruse, Failure mode and strength predictions of anisotropic bolt bearing specimens. *J. Comp. Mat.* **5**, 421–425 (1971).
2. D. W. Oplinger and K. R. Gandhi, Stresses in mechanically fastened orthotropic laminates, *2nd Conf. of Fib. Comp. in Flight Vehicle Design*, pp. 813–841 May 1974 Dayton, OH.
3. D. W. Oplinger and K. R. Gandhi, Analytical studies of structural performance in mechanically fastened fiber-reinforced plates, *Army Symp. on Solid Mech.*, pp. 211–240 Sept. 1974.
4. T. de Jong, Stresses around pin-loaded holes in elastically orthotropic or isotropic plates, *J. Comp. Mat.* **11**, 313–331 (1977).
5. T. L. Wilkinson, Stresses in the neighborhood of loaded holes in wood with applications to bolted joints, Ph.D. Dissertation, Univ. of Wisc.-Madison, Available through Univ. Microfilms (1978).
6. B. L. Agarwal, Static strength prediction of bolted joint in composite materials, *AIAA J.* **18**(11), 1371–1375 (1980).
7. P. D. Mangalgiri and B. Dattaguru, Elastic analysis of pin joints in composite plate, *Rep. No.* ARDB-STR-5014, *Dept. Aeronaut. Engr., Ind. Inst. Sci.* (1980).
8. C. M. S. Wong and F. L. Matthews, A finite element analysis of single and two-hole bolted joints in fibre-reinforced plastic, *J. Comp. Mat.* **15**, 481–491 (1981).
9. T. de Jong and H. A. Vuil, Stresses around pin-loaded holes in elastically orthotropic plates with arbitrary load direction, *Report* LR-333, *Dept. of Aerospace Engr., Delft Univ. Tech.* (1981).
10. J. H. Crews and C. S. Hong, Stress-concentration factors for finite orthotropic laminates with a pin-loaded hole, *NASA TP* 1862 (1981).
11. S. P. Garbo and J. M. Ogonowski, Effects of variances and manufacturing tolerances on the design strength of life of mechanically fastened composite joints, AFWAL-TR-81-3041, Vols. 1–3, (1981).

12. S. R. Soni, Failure analysis of composite laminates with a fastener hole, ASTM STP 749, *Joining of Composite Materials*, 145–164 (1981).
13. T. de Jong, The influence of friction on the theoretical strength of pin-loaded holes in orthotropic plates, *Rep. No.* LR-350, *Dept. of Aerospace Engr., Delft Univ. Tech.* (1982).
14. F. L. Matthews, C. M. Wong and S. Chryssafitis, Stress distribution around a single bolt in fibre-reinforced plastic, *Composites* **13**(3), 316–322 (1982).
15. R. E. Rowlands, M. U. Rahman, T. L. Wilkinson and Y. I. Chiang, Single- and multiple-bolted joints in orthotropic materials, *Composites* **13**(3), 273–278 (1982).
16. F. K. Chang, R. A. Scott and G. S. Springer, Strength of mechanically fastened composite joints, *J. Comp. Mat.* **16**, 470–494 (1982).
17. W. G. Bickley, The distribution of stress round a circular hole in a plate, *Phil. Trans. Royal Soc.* (London) **227A**, 383–415 (1928).
18. M. Nisida and H. Saito, Stress distributions in a semi-infinite plate due to a pin determined by interferometric method, *Experimental Mech.* **6**(5), 273–279 (1966).
19. N. I. Muskhelishvili, *Some Problems of the Mathematical Theory of Elasticity*, Trans. J. R. M. Radok, Noordhoff, Leyden (1977).
20. A. K. Rao, Elastic analysis of pin joints, *Computers and Structures* **9**, 125–144 (1978).
21. L. M. Milne-Thomson, *Plane Elastic Systems*, 2nd Ed., Springer-Verlag, Berlin (1968).
22. M. W. Hyer and E. C. Klang, Contact stresses in pin-loaded orthotropic plates, *CCMS Report No.* 84-02, *Dept. Engineering Science and Mechanics, Virginia Polytechnic Institute and State University* (1984).
23. S. G. Lekhnitskii, *Anisotropic Plates*, Trans. S. W. Tsai and T. Cheron, Gordon & Breach, New York (1968).
24. M. W. Hyer and D. Liu, Photoelastic determination of stresses in multiple-pin connectors, *Experimental Mech.* **23**(3), 249–256 (1983).
25. M. W. Hyer and D. Liu, Stresses in a quasi-isotropic pin-loaded connector using photoelasticity, *Experimental Mech.* **24**(1), 48–53 (1984).
26. H. B. Wilson,, Jr. and J. G. Goree, Axisymmetric contact stresses about a smooth elastic sphere in an infinite solid-stressed uniformly at infinity, *J. Applied Mech.* **34**(5), 961–966 (1967).
27. J. Dundurs and M. Comninou, An educational elasticity problem with friction, Part 1: Loading, and unloading for weak friction, *J. Applied Mechanics* **48**(4), 841–845 (1981).